Articles

Macrophage-Mediated Endothelial Inflammatory Responses to Airborne Particulates: Impact of Particulate Physicochemical Properties

Robert Kristovich,[†] Deborah A. Knight,[‡] John F. Long,[§] Marshall V. Williams,[||] Prabir K. Dutta,[†] and W. James Waldman*[,‡,||]

Departments of Chemistry, Pathology, Veterinary Biosciences, and Molecular Virology, Immunology and Medical Genetics, The Ohio State University, Columbus, Ohio 43210

Received April 15, 2004

Epidemiological studies have implicated a role for airborne particulates of <2.5 μm diameter in the development/exacerbation of chronic cardiopulmonary disease; however, specific pathogenic mechanisms and the etiological significance of particle physicochemical properties remain unresolved. Using a microporous aluminosilicate zeolite Y as a manifold, we have synthesized 1 μm particulates of pure carbon (C), carbon−iron (C/Fe), and carbon−iron/fluoro−aluminum silicate (C−Fe/F−Al−Si). We have used these particulates, as well as coal fly ash (CFA) and diesel exhaust particulates (DEP), to test the hypotheses that human macrophages treated with particulates elaborate proinflammatory cytokines in quantities sufficient to induce endothelial adhesion molecule expression and that macrophage responses to particulate exposure vary as a function of particulate physicochemical properties. Human monocyte-derived macrophages (Mø) were exposed for 24 h to sublethal concentrations of particulates, at which time phagocytosis was evident from optical microscopy. Human arterial, microvascular, or venous endothelial cells (EC) were treated with clarified supernatants recovered from Mø cultures, stained with fluorescein-conjugated mononclonal antibodies specific for endothelial adhesion molecules intercellular adhesion molecule-1, vascular cell adhesion molecule-1, or E-selectin, and assayed by fluorescence flow cytometry. Data generated by these experiments demonstrate that while supernatants of Mø exposed to CFA and C particulates are relatively ineffective, supernatants from DEP, C/Fe, or C−Fe/F−Al−Si strongly induced adhesion molecule expression on EC, responses which were completely attenuated by antibody with blocking specificity for tumor necrosis factor α. Because the only difference between C and C/Fe particulates is the presence of surface iron on C/Fe, these findings suggest particulate-induced oxidative stress as a contributing factor in Mø activation and implicate redox active iron as a major determinant of particulate bioreactivity.

Introduction

Recent epidemiological studies conducted in various geographical locations have demonstrated an association between levels of ambient airborne particulate matter and morbidity/mortality. Specific particulate-associated disease entities implicated by these studies include exacerbation of asthmatic episodes and respiratory infectious disease, chronic bronchitis, and interstitial fibrosis, as well as cardiovascular complications such as ischemic heart disease and stroke (*1*−*4*). These associations seem strongest for particulates of mass median aerodynamic diameters equal to or less than 2.5 μm ($PM_{2.5}$) (*2*−*4*). While larger size inhaled particulates (>5 μm) are likely to settle in the proximal airways where they can be trapped and cleared by ciliated epithelium, $PM_{2.5}$ can remain suspended in the pulmonary air flow, potentially reaching the alveoli where they may be retained for extended periods of time (*5*).

In vitro studies, as well as animal and human experiments, have documented a number of biological and pathological responses to particulate exposure, including enhancement of cytokine, chemokine, and intracellular oxidant production by macrophages (Møs)[1] and airway

* To whom correspondence should be addressed. Tel: 614-292-7772. Fax: 614-292-5849. E-mail: waldman.1@osu.edu.
[†] Department of Chemistry.
[‡] Department of Pathology.
[§] Department of Veterinary Biosciences.
[||] Department of Molecular Virology, Immunology and Medical Genetics.

[1] Abbreviations: Mø, macrophage; FBS, fetal bovine serum; EC, endothelial cell; SBSS, Seligman's buffered saline solution; hUVEC, human umbilical vein endothelial cell; PBS, phosphate-buffered saline; hPAEC, human pulmonary artery endothelial cell; M-CSF, monocyte colony stimulating factor; hPMVEC, human pulmonary microvascular endothelial cell; PBMC, peripheral blood mononuclear cells; TNFα, tumor necrosis factor α; LPS, lipopolysaccharide; CFA, coal fly ash; DEP, diesel exhaust particulates; C, carbon particulates; C/Fe, carbon−iron particulates; C−Fe/F−Al−Si, carbon−iron/fluouro−aluminum−silicate particulates; SEM, scanning electron microscopy; XPS, X-ray photoelectron spectroscopy.

10.1021/tx049893p CCC: $27.50
Published on Web 09/25/2004

epithelial cells following phagocytosis of particulates (*6*−*9*), impairment of chemotactic motility of particulate-laden Møs (*10*), acute and chronic pulmonary inflammation in vivo following experimental particulate administration or natural exposure in animals and humans (*11*−*14*), and the subsequent development of alveolar epithelial hyperplasia and progressive pulmonary fibrosis (*11*, *14*). Although data generated by these investigations provide some insight into possible etiological roles of inhaled particulate matter, specific mechanisms by which particulate deposition in the alveoli might initiate or exacerbate cardiopulmonary disease remain to be fully resolved.

A major focus of uncertainty resides in the relationship between the physicochemical properties of particulates and their pathogenic potential. Ambient urban airborne particulate matter consists primarily of complex mixtures of fossil fuel combustion products such as coal fly ash (CFA), residual oil fly ash, and diesel exhaust particulates (DEPs). The chemical composition of such particulates varies as a function of starting material and combustion process; however, common components include carbon aggregates, heavy metals, transition metals, acid salts, silicates, and a variety of organic compounds such as polycyclic aromatic hydrocarbons (*15*−*17*). Furthermore, the surface chemistry of particulates can be modified following their emission by reaction with atmospheric components. The etiological significance of particulate chemistry has been suggested by several studies, which have demonstrated marked differences in the biological response to particulates as a function of chemical composition and/or surface characteristics (*20*). Hence, it is of major importance to define relationships between the physicochemical properties of particulates and the mechanisms and intensity of biological responses induced following exposure.

In the current investigation, we have examined DEPs and CFA along with model 1 μm particulates composed of pure carbon (C), carbon−iron (C/Fe), or carbon−iron/fluoro−aluminum−silicate (C−Fe/F−Al−Si), with a primary focus on the role of unextractable surface iron as a determinant of bioreactivity. Considering the major roles of the Mø and the endothelium in the regulation of inflammatory responses, our biological end points involve interactions between these cell types. Specifically, we have tested the hypotheses that human Møs treated with particulates elaborate endothelial-activating cytokines in quantities sufficient to induce endothelial adhesion molecule expression and that these Mø responses to particulate exposure vary as a function of particulate physicochemical properties.

Materials and Methods

Isolation and Propagation of Endothelial Cells (EC). Human umbilical vein endothelial cells (hUVECs) were isolated from vessels as previously described (*21*). Human pulmonary artery endothelial cells (hPAECs) and human pulmonary microvascular endothelial cells (hPMVECs) were purchased from Clonetics (BioWhittaker, Walkersville, MD). hUVECs and hPAECs were propagated in endothelial cell growth medium consisting of M-199 (GibcoBRL, Grand Island, NY) supplemented with 20% fetal bovine serum (FBS, Hyclone, Logan, UT), 50 μg/mL bovine brain extract [prepared as previously described (*22*)], 12 U/mL sodium heparin (Sigma, St. Louis, MO), and 20 mM HEPES buffer. hPMVECs were propagated in EC basal medium-2 (Clonetics) supplemented with 5% FBS and the following additives as directed and supplied by the manufacturer: hydrocortisone, human fibroblast growth factor-B, vascular endothelial growth factor, insulin-like growth factor, ascorbic acid, human epidermal growth factor, and gentamycin. All growth surfaces for EC were pretreated with human fibronectin (25 μg/mL, Upstate Biotechnology, Lake Placid, NY).

The purity of all endothelial isolates was verified at passage 3 by positive immunoperoxidase staining for von Willebrand Factor and uniform negativity for leukocyte common antigen (CD45), B cell antigen (CD20), and monocyte specific antigen (CD11c) employing previously described methods (*21*). The cells were passed weekly by brief trypsin digestion at a ratio of 1:4 and used in experiments at passages 5−7.

Mononuclear Leukocyte Culture Medium. The culture medium used in the experiments, referred to as complete DMEM, consisted of DMEM (GibcoBRL), supplemented with 10% pooled human serum (from nontransfused males), 10 mM HEPES buffer, 1 mM sodium pyruvate, 1.5 mM L-glutamine, 0.6 mM L-arginine, 0.27 mM L-asparagine, 0.14 mM folic acid, 0.05 μM β-mercaptoethanol, 100 U/mL penicillin, and 100 μg/mL streptomycin.

Isolation and Differentiation of Monocytes. Peripheral blood mononuclear cells (PBMCs) were separated by Ficoll−Hypaque (Histopaque, Sigma) density gradient centrifugation (*23*) from fresh heparinized blood collected by venipuncture from healthy, nontransfused volunteers (OSU IRB-approved human subjects protocol 94HO344). PBMCs were aspirated from the plasma/Histopaque interface, washed three times in Seligman's buffered saline solution (SBSS), and suspended in complete DMEM. To promote monocyte survival, DMEM was supplemented with 10 ng/mL monocyte colony stimulating factor (M-CSF, R&D Systems, Minneapolis, MN). PBMCs were transferred to 24 well plastic tissue culture plates (Costar, Corning Inc., Corning, NY) at a concentration of $\sim 4 \times 10^6$ cells/well (1 mL/well).

The plates were incubated at 37 °C in a humidified atmosphere of 10% CO_2/90% air for 48 h to allow the adherence of monocytes. Nonadherent cells were then removed, and adherent monocytes were washed twice with SBSS and supplied with fresh complete M-CSF-free DMEM. The cells were incubated for an additional 12−14 days with medium changes at 48 h intervals to allow differentiation into the Mø phenotype.

To assess the homogeneity of populations prepared in this manner, samples were suspended by gentle scraping following 15 min of incubation in 0.01% EDTA/phosphate-buffered saline (PBS) at 4 °C and reacted for 30 min at 4 °C with 1:5 dilutions of FITC-conjugated monoclonal antibodies specific for CD3 and CD14 (Gen Trak, Liberty, NC). The stained cells were washed twice, suspended in cold SBSS, and analyzed (5000 cells) using a Coulter Epics XL flow cytometer. As controls for nonspecific staining, the cells were reacted with appropriate isotypically matched irrelevant murine antibodies. Cells prepared in this manner were routinely marked 90−95% positive for CD14 with undetectable levels of T cell contamination (as indicated by the absence of $CD3^+$ cells).

Synthesis/Preparation of Particulates. The procedures described here are an adaptation of a previously published procedure for the synthesis of a carbonaceous negative image of a zeolite (*24*). The synthesis of carbon particle replicas proceeds through an acid-catalyzed condensation reaction of phenol and paraformaldehyde monomers using zeolite Y as a template for the reaction. The zeolite was acidified by ion exchange with NH_4Cl, followed by decomposition of the ion-exchanged ammonium ions under vacuum at 500 °C. For the synthesis of C/Fe and C−Fe/F−Al−Si particulates, iron was added by ion exchange with 0.01 M ferrous sulfate (3 cycles, 30 min/cycle) before decomposition of the ammonium ions. The zeolite was cooled to room temperature, and solid phenol (0.21 g phenol/g zeolite) was added. A weak vacuum was pulled on the system, and the temperature was raised slowly to 60 °C. Solid paraformaldehyde (0.25 g paraformaldehyde/g zeolite) was added to the zeolite/phenol material, and the temperature was

raised very slowly to 120 °C in a nitrogen environment. At this point, the solid material turned red as the phenol/paraformaldehyde cross-linked polymer formed. The solid material was held at 120 °C for 5 h to allow for complete polymerization. The zeolite/polymer mix was pyrolyzed at 800 °C for 19 h under flowing argon. The zeolite template was removed by etching in 48% hydrofluoric acid for 6 h. For making the C−Fe/F−Al−Si particulates, the solubilized aluminum and silicate of the zeolite template were reprecipitated on the C/Fe particles.

CFA (up to 100 μm mass median aerodynamic diameter) was acquired from a coal-burning electric power plant and was size fractionated to <2.5 μm by sedimentation in water. The fly ash was suspended in a 10 cm column of H_2O and allowed to settle for 1 h, followed by recovery and filtration of the supernatant. DEPs were recovered from the exhaust pipe of a diesel-powered truck.

Characterization of Particulates. The surface chemical composition was determined on a Kratos Ultra Axis XPS using an aluminum source. Carbon, carbon/iron, and diesel were conductive and therefore required no charge balancing. C−Fe/F−Al−Si and CFA were found to be insulating and therefore required charge balancing of 2.1 and 2.6 V, respectively. Survey scans were performed with pass energy of 80 eV, and high-resolution scans of the individual component regions were performed with pass energy of 20 eV. The individual component concentrations were determined by averaging 10 scans and determining the area under each component peak; after, a Shirley baseline correction algorithm was performed (*25*). The areas were normalized using elemental sensitivity factors, obtained from the software package of the Kratos Ultra Axis system. Scanning electron micrographs were recorded on gold-coated samples on a Phillips XL-30 ESEM, operating at 12 kV accelerating current. The crystallinity of all particles was determined by analyzing the powder diffraction pattern obtained on a Rigaku Geigerflex powder X-ray diffractometer.

Treatment of Møs with Particulates. Particulates were sterilized by steam autoclave and suspended in serum-free DMEM at a concentration of 5 μg/mL. Møs differentiated in culture plates as described above were washed with PBS and supplied with fresh DMEM (0.5 mL/well). Particulates were sonicated and immediately added to Mø cultures within concentration ranges determined to be nontoxic by trypan blue dye exclusion (C, 5−50 μg/cm^2; C/Fe, C−Fe/F−Al−Si, and DEP, 2.5−25 μg/cm^2; CFA, 10−100 μg/cm^2). Because certain of these particulates settle more slowly through the culture medium, notably C and DEP, all plates were centrifuged for 10 min at 300*g* immediately following the addition of particulates. While this step was not necessary for the induction of effects described below, it did serve to equilibrate the time of initial particulate contact with Mø.

Assay of Mø-Mediated Endothelial Activation. To determine the impact of soluble factors elaborated by particulate-exposed Mø upon proximal endothelia, ECs were incubated with supernatants recovered from particulate-laden Mø cultures and then assayed by immunofluorescence flow cytometry for expression of endothelial leukocyte adhesion molecules. Replicate experiments were conducted with human EC derived from umbilical vein (hUVEC), pulmonary artery (hPAEC), and pulmonary microvasculature (hPMVEC), and with Mø isolated from five individual healthy volunteer donors (2−4 replicate experiments per donor). Møs differentiated in 24 well culture plates for 10−12 days were treated with nontoxic concentrations of particulates as described above. Following 24 h of incubation, at which time phagocytosis of all particulates was clearly evident (see Figure 6), supernatants were recovered from particulate-treated or untreated Mø, clarified by centrifugation, and overlaid upon confluent monolayers of hUVEC, hPAEC, or hPMVEC in 24 well culture plates. Additional controls included untreated quiescent EC, EC treated with 300 IU/mL human recombinant tumor necrosis factor α (TNFα, R&D Systems) as a positive control for adhesion molecule induction, and ECs treated with clarified lysates of sonicated Mø. The plates were incubated at 37 °C in a humidified atmosphere of 10% CO_2/90% air for 4, 8, or 24 h and then harvested by brief trypsin digestion for assay of induction of E-selectin, vascular cell adhesion molecule (VCAM)-1, and intercellular adhesion molecule (ICAM)-1, respectively.

The cells were suspended in SBSS and reacted for 30 min at 4 °C with FITC-conjugated monoclonal antibodies specific for E-selectin (Ancell Corp., Bayport, MN, 1:50 dilution), VCAM-1 (Ancell, 1:100 dilution), or ICAM-1 (Gen Trak, 1:100 dilution). The stained cells were washed twice, suspended in cold SBSS, and analyzed (5000 cells) using a Coulter Epics XL flow cytometer. As antibody controls, the cells were reacted with appropriate isotypically matched irrelevant murine antibodies.

To specifically identify the inducing agent produced by particulate-treated Møs, supernatants recovered from Mø cultures were incubated for 1 h with 0.25 μg/mL polyclonal rabbit anti-human TNFα (Genzyme Diagnostics, Cambridge, MA) or with 0.25 μg/mL irrelevant polyclonal rabbit IgG (Jackson Immunoresearch Laboratories, West Grove, PA) prior to addition of supernatants to endothelial monolayers.

To determine if Mø responses were due to endotoxin, which may have been brought into cells on the particulates, a subset of the experiments described above were performed in the presence of polymyxin B (Sigma). Aliquots of each particulate suspension were supplemented with polymyxin B at a concentration of 10 μg/mL (shown to effectively neutralize the effects of 100 pg/mL lipopolysaccharide [LPS, Sigma]). Because the volume of particulate suspensions added to culture wells was small (2−40 μL), the culture medium in wells was supplemented with polymyxin B (10 μg/mL) prior to the addition of particulates.

Results

Description of Particulates. The basic synthetic strategy for making the model C particulates was to start with ∼1 μm size microporous aluminosilicate zeolites and synthesize a polymer within the zeolite cavities. The zeolite−polymer composite was then heated to 800 °C to graphitize the carbon. With the use of HF, the aluminosilicate framework was dissolved, leaving behind the carbon particle. Figure 1a shows the scanning electron microscopy (SEM) of C particles synthesized by the above method, and it is indistinguishable from the starting zeolite (Figure 1c). The surface elemental analysis (Figure 1b) as determined by X-ray photoelectron spectroscopy (XPS) shows mostly carbon with a small contribution from silicon and no peak due to aluminum. Table 1 lists the elemental analysis as determined by XPS. The C particles were amorphous.

To make C/Fe, the starting zeolite was ion-exchanged with Fe^{3+} and the synthesis process was repeated. Figure 2 shows the SEM and XPS. The morphology, as expected, is very similar to the C particle, but as the XPS indicates, Fe^{3+} is incorporated into the particle, as seen in the inset of Figure 2b. The surface iron loading was calculated from the XPS to be 1.8% by mass, as shown in Table 1.

A third model particle was prepared, in which the aluminosilicate framework was dissolved by the HF, but instead of separating the dissolved aluminosilicate from the C particles, it was reprecipitated by treatment with ammonium hydroxide. We refer to these particles as C−Fe/F−Al−Si, and they were synthesized to impart charge onto the hydrophobic C particles. Figure 3 shows the SEM and XPS of the C−Fe/F−Al−Si particles, and Table 1 lists the surface composition. Because of the strong peak due to F, the Fe peak could not be distinguished from the XPS, so a bulk analysis was done on the sample and found to contain 2 wt % iron. Figure 3c

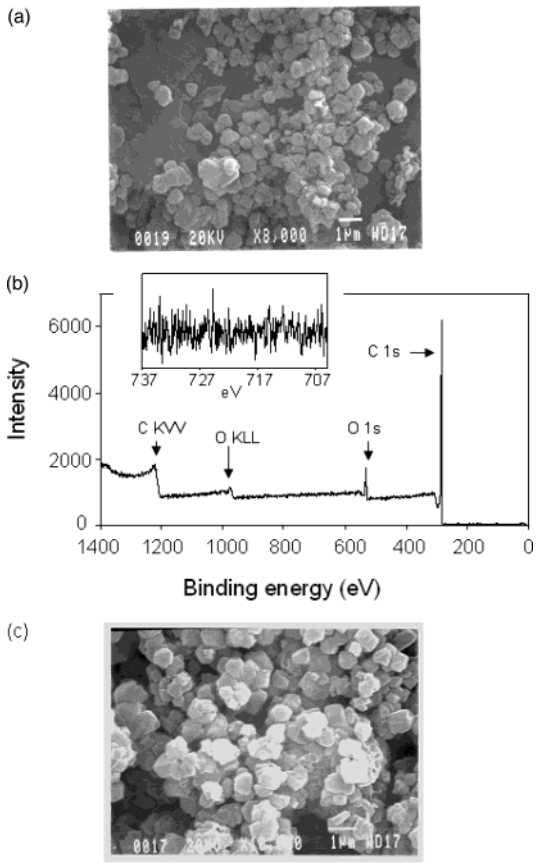

Figure 1. Characteristics of the C particles: (a) SEM, (b) XPS (inset is the iron region), and (c) SEM of the starting zeolite Y.

Table 1. Surface Mass Concentrations as Determined by XPS (ND = Not Detected)

element	C (% by mass)	C/Fe (% by mass)	C−Fe/F−Al−Si (% by mass)	CFA (% by mass)	diesel (% by mass)
carbon	88.1	79.9	19.9	25.4	70.3
iron	ND	1.8	ND (F peak)	3.0	3.0
aluminum	ND	ND	5.5	13.3	ND
silicon	0.9	2.2	3.4	16.7	ND
fluorine	ND	ND	50.4	ND	ND
oxygen	10.0	16.1	6.4	41.1	24.0
nitrogen	1.0	ND	10.9	0.5	1.0
sulfur	ND	ND	ND	ND	1.7
sodium	ND	ND	3.5	ND	ND
potassium	ND	ND	ND	trace	ND

is the powder X-ray diffraction pattern (XRD) of the C−Fe/F−Al−Si, and unlike the C and C/Fe particles, it appeared to be crystalline, and the diffraction pattern matched well to a mixture of $(NH_4)_3AlF_6$ and $(NH_4)_2SiF_6$ (*26*, *27*).

Two ambient particles of interest in this study were CFA and DEPs. Figure 4 shows the SEM, XPS, and XRD of the CFA. The size-fractionated CFA is <2 μm in diameter and was crystalline, as evident from Figure 4c. The surface elemental analysis shows an aluminosilicate particle with iron. The crystalline components in CFA were identified to be primarily quartz and mullite and are marked in Figure 4c. The spherical morphology of the particles (also called cenospheres) is characteristic of CFA and originates during coal combustion due to gas bubbles trapped inside the particles (*28*).

Figure 5 shows the SEM and XPS of the DEPs. These are ~150 nm particles, with C as the major component and minor quantities of iron and sulfur (Table 1) and resembles the C/Fe in surface composition.

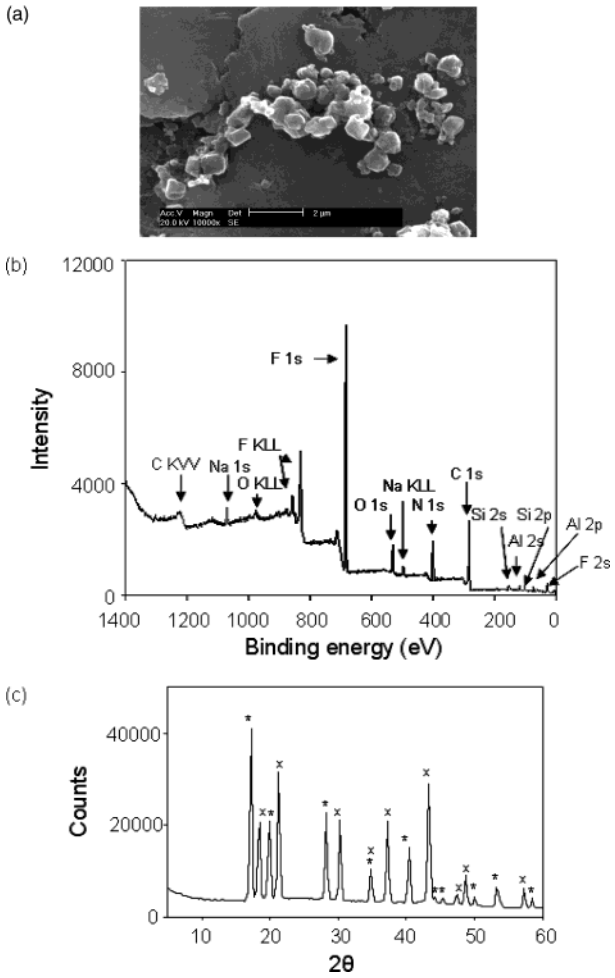

Figure 3. Characteristics of the C−Fe/F−Al−Si particles: (a) SEM, (b) XPS, (c) powder X-ray diffraction [* = $(NH_4)_3AlF_6$ and x = $(NH_4)_2SiF_6$].

Phagocytosis and Toxicity of Particulates. We first sought to determine the extent of phagocytosis and relative toxicities of the environmental particulates and those that we had synthesized. Human peripheral blood monocytes were allowed to differentiate in vitro for 10−12 days into the Mø phenotype and were then treated with various concentrations of particulates and studied by phase contrast microscopy. As shown in Figure 6, all particulates were readily phagocytosed by Mø within 24 h. As determined by trypan blue dye exclusion and morphologic evidence of cell degeneration, the particulates exhibited a range of toxicities as a function of particulate physicochemical characteristics. While the synthesized C−Fe/F−Al−Si particulates were toxic at concentrations greater than 40 μg/cm^2, no toxicity was apparent in Mø treated with up to 200 μg/cm^2 of CFA or synthesized C particulates. DEP and synthesized C−Fe exhibited intermediate toxicities in the range of 50−70 μg/cm^2 (data not shown).

Møs treated with concentrations of particulates below toxic levels were periodically stained with trypan blue and carefully observed for morphologic indicators of apoptosis and necrosis. No evidence of cell death was observed in these populations for over 4 weeks following particulate exposure.

Mø-Mediated Endothelial Activation. To determine the impact of soluble factors elaborated by particulate-

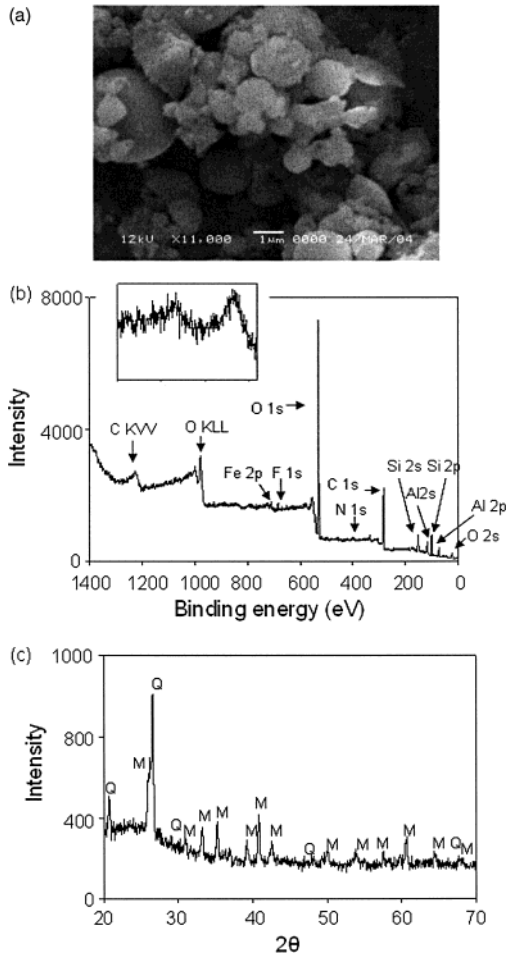

Figure 4. Characteristics of the CFA particles: (a) SEM, (b) XPS (inset is the iron region, with the peaks due to Fe^{3+} marked), and (c) powder X-ray diffraction (Q = quartz; M = mullite).

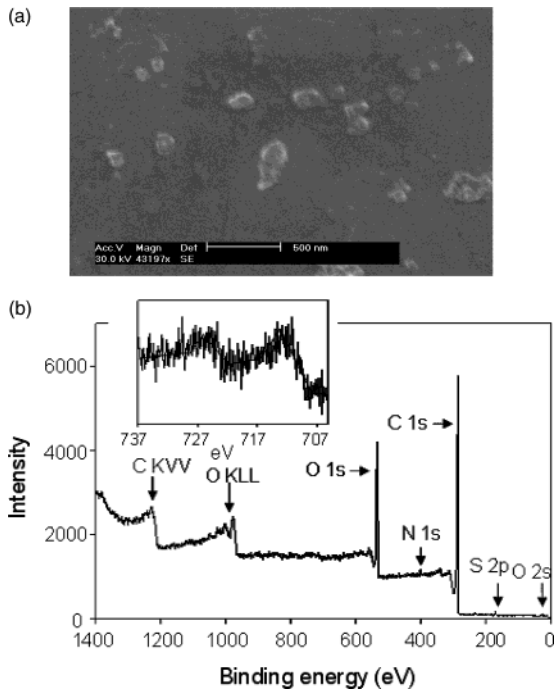

Figure 5. Characteristics of the DEP: (a) SEM and (b) XPS (inset is the iron region, with the peaks due to Fe^{3+} marked).

exposed Møs upon proximal endothelia, human ECs derived from umbilical vein (hUVEC), pulmonary artery

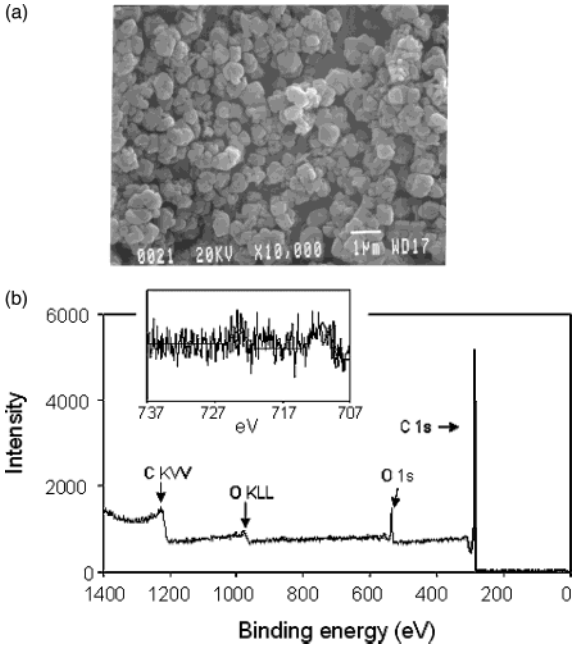

Figure 2. Characteristics of the C/Fe particles: (a) SEM and (b) XPS (inset is the iron region, with the peaks due to Fe^{3+} marked).

(hPAEC), or pulmonary microvasculature (hPMVEC) were incubated with supernatants recovered from particulate-treated human Mø cultures and then assayed by immunofluorescence flow cytometry for expression of endothelial leukocyte adhesion molecules. Shown in Figure 7 is a representative series of flow cytometric histograms demonstrating responses of hPAEC following 4 (E-selectin), 8 (VCAM-1), or 24 h (ICAM-1) of incubation with supernatants recovered from C/Fe-treated Mø (25 $\mu g/cm^2$). These incubation times are based upon numerous studies, which demonstrate that ECs treated with TNFα, a known product of activated Mø, express peak levels of E-selectin at 4 h, which rapidly wane, peak levels of VCAM-1 at 8 h, which wane more slowly, and peak levels of ICAM-1 at 24 h, which are sustained for several days (*29*). As shown in the figure, untreated quiescent hPAECs express modest constitutive levels of surface ICAM-1 but no detectable VCAM-1 or E-selectin. While supernatants recovered from untreated Mø had no effect on endothelial adhesion molecule expression, supernatants recovered from C/Fe-treated Mø enhanced surface ICAM-1 expression and induced surface expression of both VCAM-1 and E-selectin. Nonspecific staining with irrelevant isotype-matched control antibodies was negligible under all conditions (data not shown).

Figure 8 presents data generated by immunofluorescence flow cytometric analysis of ICAM-1, VCAM-1, and E-selectin surface expression on hPMVEC following incubation with supernatants recovered from untreated Mø (DMEM) or supernatants recovered from Mø treated with various concentrations of each of the five types of 1 μm particulates (C, C/Fe, C−Fe/F−Al−Si, DEP, and CFA). Mean fluorescence intensity (MFI) values shown in the figure were calculated by subtracting MFI generated by nonspecific staining with irrelevant isotype-matched control antibodies from MFI of specifically stained cells. These curves demonstrate dose-dependent induction of all three adhesion molecules upon hPMVEC incubated with supernatants recovered from Møs treated with C/Fe, C−Fe/F−Al−Si, or DEP. (Because toxic effects

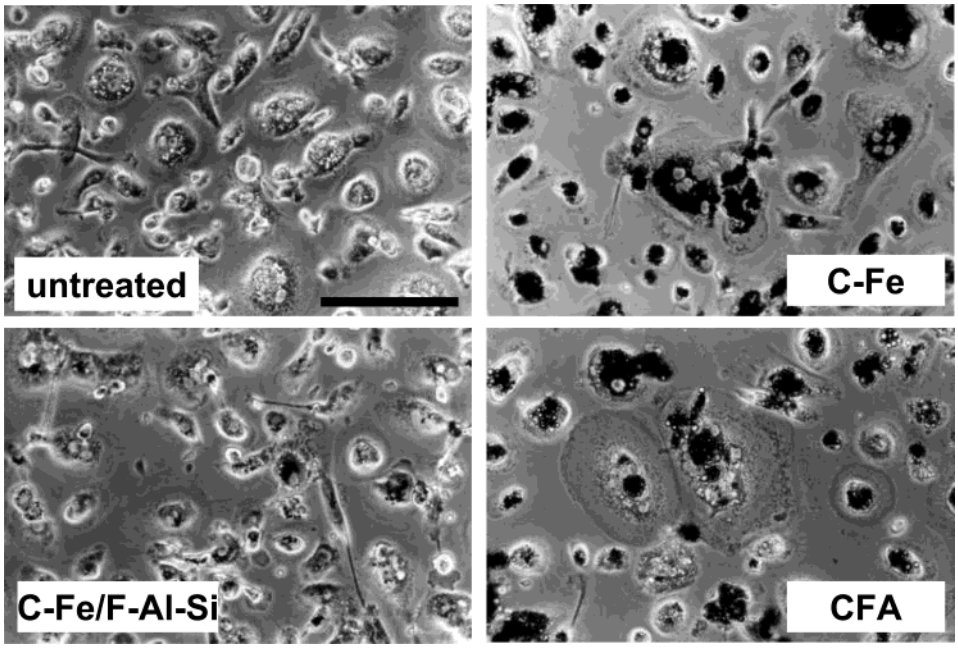

Figure 6. Phase contrast micrographs of untreated human peripheral blood monocyte-derived Møs, Mø incubated for 24 h in the presence of synthesized 1 μm C/Fe (25 μg/cm^2 surface area) or C−Fe/F−Al−Si (12.5 μg/cm^2), or Mø incubated for 24 h in the presence of size-fractionated (≤2.5 μm) CFA (25 μg/cm^2). Bar = 100 μm.

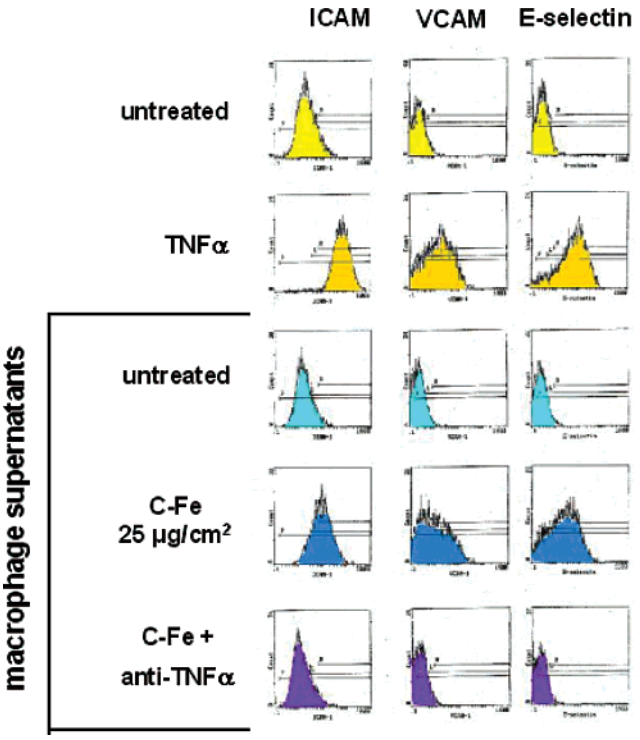

Figure 7. Immunofluorescence flow cytometric analysis of Mø-mediated endothelial adhesion molecule induction by synthesized 1 μm C/Fe. hPAECs were either untreated, incubated in the presence of TNFα (300 IU/mL), incubated in supernatants recovered from cultures of untreated Møs or Mø exposed for 24 h to C/Fe (25 μg/cm^2), or incubated in the presence of supernatants of C/Fe-treated Mø and antibody with specific blocking activity against TNFα (anti-TNFα). hPAECs were then stained with FITC-conjugated monoclonal antibodies specific for ICAM-1, VCAM-1, or E-selectin and analyzed by fluorescence flow cytometry (5000 cells/sample).

induced by these particulates upon Mø began to occur at concentrations of 40−50 μg/cm^2, curves generated by these particulates terminate at 25 μg/cm^2.) In contrast, little or no endothelial activation was observed in response to supernatants recovered from Møs treated with C or CFA, even at 2−4-fold greater concentrations. Data generated by these experiments suggest that the inflammatory potential of phagocytosed particulates varies greatly as a function of particulate physicochemical characteristics.

These data are representative of experiments performed with Mø isolated from each of five volunteer donors (2−4 replicate experiments/donor) and with human endothelial cells derived from umbilical vein, pulmonary artery, and pulmonary microvasculature. We have previously demonstrated that endothelial responses to TNFα and interferon-γ are qualitatively and quantitatively similar regardless of vascular bed of origin (*30*, *31*). Replicate experiments conducted with hPMVEC, hUVEC, and hPAEC demonstrated that while the magnitude of endothelial responses varied among experiments, the pattern of particulate-induced responses remained constant, and no correlation between the magnitude of responses and the origin of the EC was observed.

Rather the variation in magnitude of particulate-induced responses was more closely related to the source of the Mø, i.e., the PBMC donors. Figure 9 presents data generated by immunofluorescence flow cytometric analysis of ICAM-1 (A), VCAM-1 (B), and E-selectin (C) surface expression on hPMVEC following incubation with supernatants recovered from untreated Mø (DMEM) or supernatants recovered from Mø treated with maximally inducing concentrations of each of the five types of 1 μm particulates (C, C/Fe, C−Fe/F−Al−Si, DEP, and CFA). MFI values shown in the figure were normalized to MFI values generated by EC incubated with supernatants recovered from untreated Mø. These data demonstrate that while the magnitude of endothelial adhesion molecule induction varies among Mø donors, the pattern of induction remains essentially constant. In all experiments, C/Fe, C−Fe/F−Al−Si, and DEP were observed to induce Mø-mediated endothelial activation, whereas C

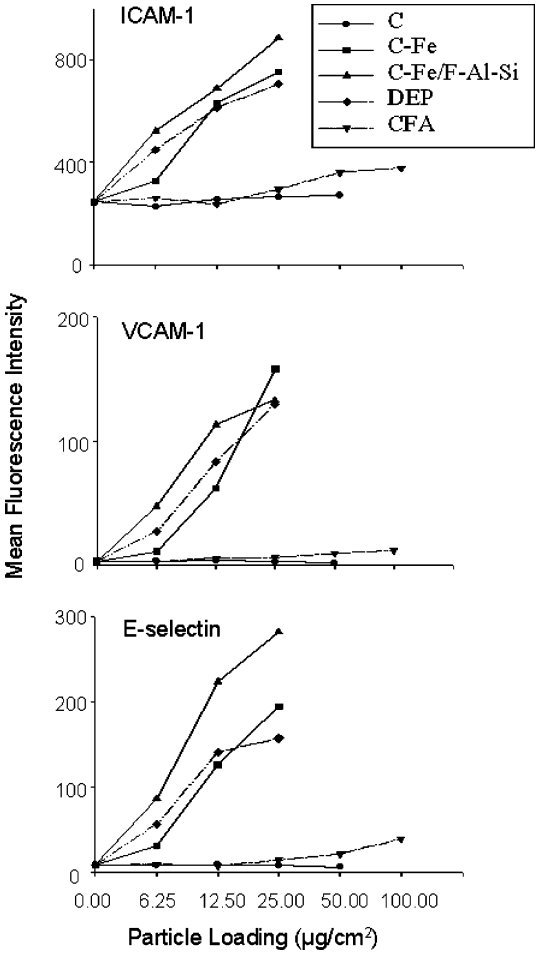

Figure 8. Immunofluorescence flow cytometric analysis of Mø-mediated endothelial adhesion molecule induction by synthesized and environmental particulates. hPMVECs were incubated with supernatants recovered from cultures of untreated Møs or from cultures of Mø exposed for 24 h to various concentrations of 1 μm synthesized C, C/Fe, or C−Fe/F−Al−Si or from cultures of Mø exposed for 24 h to DEP or size-fractionated CFA. hPMVECs were then stained with FITC-conjugated monoclonal antibodies specific for ICAM-1, VCAM-1, or E-selectin and analyzed by fluorescence flow cytometry (5000 cells/sample). Because toxic effects induced by C/Fe, C−Fe/F−Al−Si, or DEP upon Mø began to occur at concentrations of 40−50 μg/cm^2, curves generated by these particulates terminate at 25 μg/cm^2.

and CFA appeared relatively inert in the context of the measured responses. It should also be noted that even Møs isolated from the same individual, but at different times, demonstrated variation in response magnitude, likely as a consequence of donor immune status at the time blood was drawn (subclinical infection, convalescence from a recent infection, stress level, etc.). Despite this variation, endothelial activation by "high" responders (Figure 9, donor 1) generally remained high, and activation by "low" responders (Figure 9, donor 2) generally remained low.

To control for the possibility that normal Mø products released simply as a consequence of cell injury might induce this endothelial activation, ECs were also treated with clarified lysate of sonicated untreated Mø. No adhesion molecule induction was observed in response to this treatment (Table 2).

To determine if Mø responses were elicited by endotoxin, which may have been brought into cells on the particulates, a subset of the experiments described above

Table 2. Mean Fluorescence Intensities Generated by Flow Cytometric Analysis of ICAM-1, VCAM-1, and E-selectin Expression on hPMVEC Following Incubation with Supernatants of Untreated Møs, Lysed Mø, or Mø Exposed for 24 Hours to Maximally Inducing Concentrations of 1 μm Synthesized Particulates of Pure Carbon (C), Carbon−Iron (C−Fe), Carbon−Iron/Fluoro-aluminum Silicate (C−Fe/F−Al−Si), DEP, or Size-fractionated CFA, in the Presence or Absence of 10 μg/mL Polymyxin B (polyB)

	mean fluorescence intensity		
treatment	ICAM-1	VCAM-1	E-selectin
none	132	2.5	5.4
TNFα	957	186	308
Mø supernatants			
untreated	195	1.6	6.3
lysed	216	1.9	5.7
polyB	179	1.2	7.1
LPS[a]	746	141	258
LPS + polyB	183	2.1	6.9
C (50[b])	247	2.8	4.9
C (50[b]) + polyB	263	2.3	5.6
C/Fe (25[b])	786	139	218
C/Fe (25[b]) + polyB	802	131	211
C−Fe/F−Al−Si (25[b])	878	152	232
C−Fe/F−Al−Si (25[b]) + polyB	859	158	242
DEP (25[b])	726	127	187
DEP (25[b]) + polyB	748	138	183
CFA (100[b])	351	9.9	32
CFA (100[b]) + polyB	359	9.1	38

[a] LPS (100 pg/mL). [b] μg/cm^2.

were performed in the presence of 10 μg/mL polymyxin B, a known inactivator of endotoxin. While this concentration of polymyxin B in Mø cultures completely neutralized endothelial adhesion molecule induction by supernatants recovered from Mø stimulated by 100 pg/mL of LPS, it did not attenuate adhesion molecule induction by particulate-treated Mø supernatants (Table 2).

Because TNFα is known to be produced by activated Mø and is also known to induce endothelial ICAM-1, VCAM-1, and E-selectin (*29*), we sought to verify the identity of the inducing factor(s) elaborated by particulate-treated Mø. Supernatants recovered from Mø cultures were incubated for 1 h with polyclonal antibody with blocking activity specific for TNFα (0.25 μg/mL) or with equal concentrations of irrelevant control polyclonal IgG prior to addition of supernatants to endothelial monolayers. As shown in Figure 7, induction of all three adhesion molecules by C/Fe-treated Mø supernatants was completely neutralized by anti-TNFα but not by irrelevant control antibody (data not shown). Complete neutralization of endothelial activation by anti-TNFα was also observed in EC incubated with supernatants recovered from Mø treated with C−Fe/F−Al−Si, DEP, and CFA (data not shown).

Discussion

Despite considerable effort expended in the investigation of biological interactions of airborne particulate matter, numerous questions remain regarding specific pathogenic mechanisms by which inhaled particulates might exacerbate respiratory infections, asthmatic episodes, chronic bronchitis, and interstitial fibrosis, as well as cardiovascular complications such as ischemic heart disease and stroke (*1*−*4*). Several mechanisms have been proposed to explain the inflammatory response to par-

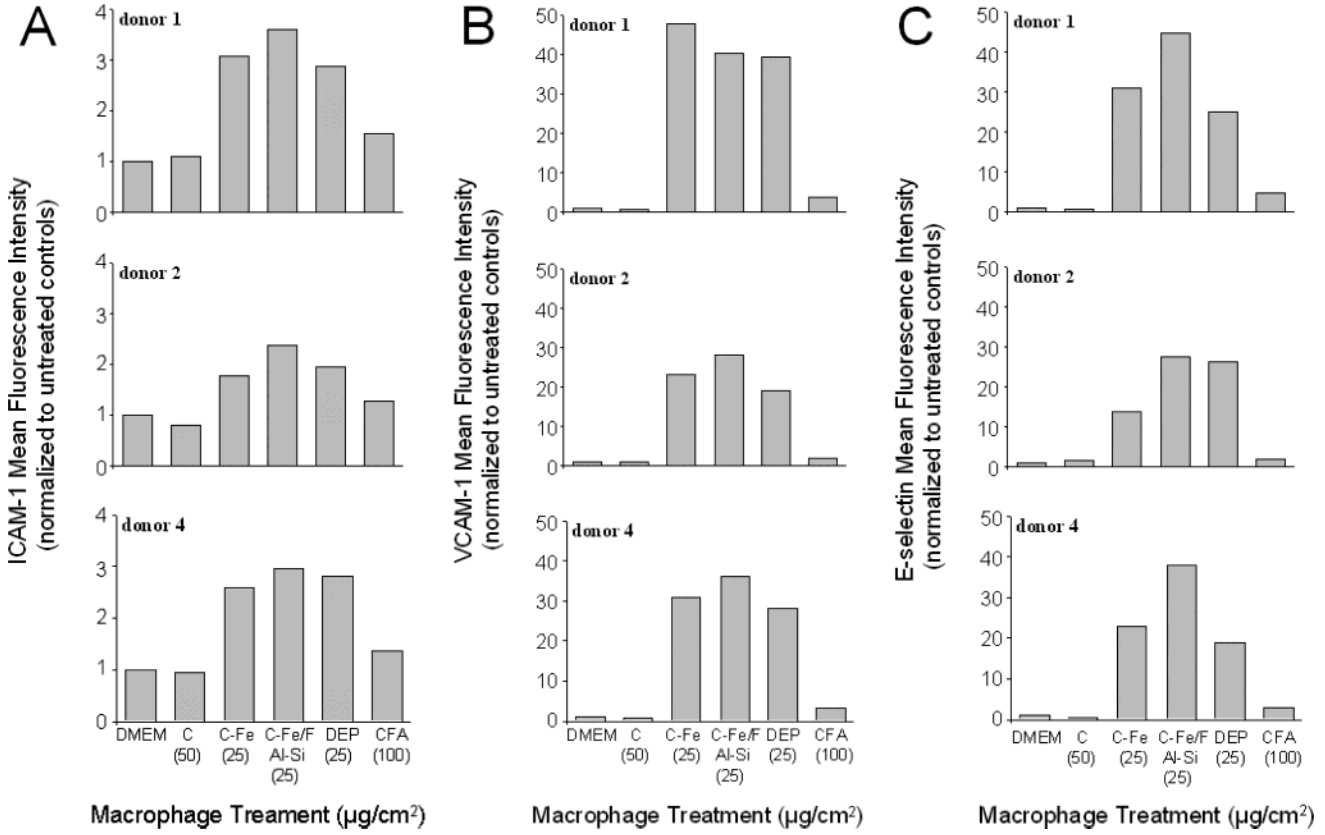

Figure 9. Mø donor-dependent variation in magnitude of inflammatory responses to synthesized and environmental particulates. hPMVECs were incubated with supernatants recovered from cultures of untreated Møs isolated from three individual donors (DMEM) or from cultures of Mø exposed for 24 h to maximally inducing concentrations of 1 μm synthesized C, C/Fe, and C−Fe/F−Al−Si or from cultures of Mø exposed for 24 h to DEP or size-fractionated CFA. hPMVECs were then stained with FITC-conjugated monoclonal antibodies specific for ICAM-1 (A), VCAM-1 (B), or E-selectin (C) and analyzed by fluorescence flow cytometry (5000 cells/sample). Mean fluorescence intensity values were normalized to values generated by supernatants of untreated Mø.

ticulate exposure including direct alveolar epithelial cell injury (*10*, *18*), accumulation of particulates within the septal interstitium (*32*), and induction of inflammatory mediator production by alveolar epithelial cells and Møs (*6*−*9*). However, the endothelium has received little attention in this regard. Once considered a complacent barrier with the assumed primary function of inhibition of aberrant intravascular thrombosis, the endothelium has emerged as a dynamically interactive participant in immunomodulation. In particular, the microvascular endothelium is of central importance in the regulation of inflammation by virtue of its ability to inducibly express endothelial leukocyte adhesion molecules (*33*). Under normal circumstances, ECs remain in a quiescent state, expressing modest levels of ICAM-1, no E-selectin, and (with the exception of limited subsets) no VCAM-1. However, under inflammatory conditions, as a consequence of cytokine interactions, EC are induced to express VCAM-1 and E-selectin, as well as enhanced levels of ICAM-1 (*29*), providing a substrate for adherence, activation, and extravasation of circulating neutrophils, monocytes, and lymphocytes.

A major source of endothelial-activating cytokines, particularly TNFα, is the activated tissue Mø (*29*). Forces that activate these cells, such as microorganisms and various toxins, provide the stimulus for the recruitment of inflammatory cells to the site of injury. The alveoli contain resident Møs, which increase in number with increasing intraalveolar particulate load. The alveolar capillary endothelium is separated from the alveolar Mø by only a monolayer of flattened alveolar epithelium and a thin basal lamina, a total distance of ∼150−200 nm, which is easily traversed by soluble factors produced in the alveoli.

In the current investigation, we have assessed the impact of synthetic C, C/Fe, and C−Fe/F−Al−Si particulates upon Mø-mediated endothelial inflammatory responses, comparing responses to the synthetic particulates with those elicited by size-fractionated (≤1 μm) CFA and DEP.

The etiological significance of particulate chemical composition and surface characteristics is evident from the fact that even though all particulates were readily phagocytosed by Mø, the effectiveness of the particulates in inducing the inflammatory effect varied dramatically with their chemical composition and surface properties. While relatively low concentrations of C/Fe, C−Fe/F−Al−Si, and DEP stimulated endothelial adhesion molecule expression (through Mø production of TNFα), little or no effect was detected with C or CFA, even at loadings of particles several times greater.

In particular, considering that the only difference between the C and the C/Fe particles is the presence of surface iron on C/Fe, with all other features including the morphology of the particles being very similar, it can be unequivocally stated that the Mø-mediated induction of endothelial adhesion molecule expression by C/Fe must be due to the surface iron. There are several features that we can associate with the iron on C/Fe. It is present as Fe^{3+} and will not be readily solubilized, since the synthesis of the particles involved treatment with concentrated HF to dissolve the aluminosilicate framework.

Thus, the biological manifestation must arise from the surface bound redox chemistry of iron. The fact that solubilized iron can lead to the formation of hydroxyl radical by the Fenton reaction is well-recognized, and iron-containing particles are proposed as a mechanism to introduce iron into cells, bypassing normal regulatory controls of iron transport. Increasingly though, there is awareness that the chemistry of the iron attached to the particle surface may also be biologically relevant (*34*), as we have also noted for iron-exchanged erionite and mordenite (*35*). Unregulated soluble iron has long been linked to an increase in oxidative stress in cellular systems (*36*, *37*). The Fenton reaction is a route to make reactive oxygen species as follows:

$$Fe^{3+} + H_2O_2 \rightarrow Fe^{2+} + HO_2^{\bullet} + H^+ \quad (1)$$

$$Fe^{2+} + H_2O_2 \rightarrow Fe^{3+} + OH^- + OH^{\bullet} \quad (2)$$

In addition to H_2O_2, other possible biological reductants include ascorbic acid and glutathione.

Several studies have implicated a role for iron in promoting gene expression resulting in increased formation of proinflammatory mediators. In particular, soluble iron (Fe^{2+}) has been shown to induce expression of TNFα in cultured Kupffer cells via the NF-κB pathway, the activation of which was directly preceded by an increase in paramagnetic resonance detectable •OH (*38*). Consistent with these observations, iron chelators have been shown to inhibit NF-κB activation in hepatic Møs (*39*). However, the specific molecular mechanisms by which hydroxyl radicals regulate NF-κB activation remain to be resolved.

The role of surface iron in promoting Mø-mediated endothelial activation by C/Fe particles is consistent with the similar response elicited by DEP, which, based on the XPS, are particles with a carbon core and surface iron. The source of iron is presumably from the metallic parts of the combustion and exhaust process. The enhanced endothelial activation level induced by C−Fe/F−Al−Si as compared to the C/Fe or DEP is also of interest. The major difference between C/Fe and C−Fe/F−Al−Si is the presence of negatively charged species (aluminum and silicon fluorides). An increased negative charge on environmental particulates has been reported to enhance the release of inflammatory cytokine IL-6 in cultured human respiratory epithelial cells (*40*).

However, the CFA particles also have a surface charge (aluminosilicate) and significant levels of surface iron; yet, their bioactivity in the context of our experiments is slightly higher than the inactive C particles but with a doubled loading level. Typically, the iron present in coal is in the form of pyrite. Upon combustion at high temperatures, the pyrite loses the sulfur and the iron ends up as oxides or incorporated into the aluminosilicate framework (*41*). Even though elemental analysis shows high levels of iron in the CFA, no distinct phases due to iron could be distinguished in the diffraction patterns. Previous studies have shown that CFA promoted the formation of the cytokine IL-8 in human lung epithelial cells, and solubilized iron from CFA was thought to be responsible (*42*). Other studies have shown that CFA was considerably poorer in eliciting TNF production as compared to coal and silica dusts (*43*). The bioavailabilty of iron from CFA has been noted to depend on the particle size and the type of coal (*44*), and that makes it difficult to compare different studies. The size of the CFA in this study is in the range (<2.5 μm), and it has been noted that the iron in the glassy phase is higher with smaller particles (*44*). If CFA were not releasing iron, then, in order for Fenton chemistry to be active, the surface iron would have to play a role. For the iron present in the surface as iron oxides, the biological activity is expected to be minimal as noted for hematite and magnetite (*45*). For the iron present in the aluminosilicate to be bioactive, both redox chemistry and coordination sites around iron are necessary (*46*), which may not occur readily for the iron incorporated in the glassy phase of CFA.

In summary, the data presented here support the hypothesis that surface chemistry of particulates, especially as manifested by the redox chemistry of iron, has a significant impact upon the consequent biological response. Specifically, our results suggest that the presence of iron on the surface of particulates phagocytosed by Møs exerts intracellular oxidative stress leading to enhanced expression and release of TNFα. In the context of the pulmonary microenvironment, TNFα elaborated by particulate-laden alveolar Møs could act upon proximal septal capillary endothelial cells, inducing their expression of endothelial leukocyte adhesion molecules ICAM-1, VCAM-1, and E-selectin, and thus promoting localized inflammatory responses. In addition, results of this study demonstrate the utility of simplified synthetic model particulates in the elucidation of particulate properties which determine their bioreactivity. In particular, comparison of the C and C/Fe particles suggests that the iron does not need to be in a solubilized form, implying that smaller particles with a greater surface area would have a more pronounced biological activity.

Acknowledgment. This work was funded in part by NSF Grant CHE-0089147 and NSF-DMR 0114098.

References

(1) Dockery, D. W., Pope, C. A., III, Xu, X., Spengler, J. D., Ware, J. H., Fay, M. E., and et al. (1993) An association between air pollution and mortality in six U.S. cities. *N. Engl. J. Med. 329*, 1753−1759.

(2) Koenig, J. Q., Larson, T. V., Hanley, Q. S., Rebolledo, V., Dumler, K., Checkoway, H., and et al. (1993) Pulmonary function changes in children associated with fine particulate matter. *Environ. Res. 63*, 26−38.

(3) Ilabaca, M., Olaeta, I., Campos, E., Villaire, J., Tellez-Rojo, M. M., and Romieu, I. (1999) Association between levels of fine particulate and emergency visits for pneumonia and other respiratory illnesses among children in Santiago, Chile. *Air Waste Manage. Assoc. 49*, 154−163.

(4) Pope, C. A. III, Burnett, R. T., Thun, M. J., Calle, E. E., Krewski, D., Ito, K., and et al. (2002) Lung cancer, cardiopulmonary mortality, and long-term exposure to fine particulate air pollution. *J. Am. Med. Assoc. 287*, 1132−1141.

(5) Anderson, M., Svartengren, M., Philipson, K., and Camner, P. (1988) Regional human lung deposition studied by repeated investigations. *J. Aerosol Sci. 19*, 1121−1124.

(6) Finkelstein, J. N., Johnston, C., Barrett, T., and Oberdörster, G. (1997) Particulate-cell interactions and pulmonary cytokine expression. *Environ. Health Perspect. 105*, 1179−1182.

(7) Goldsmith, C. A., Imrich, A., Danaee, H., Ning, Y. Y., and Kobzik, L. (1998) Analysis of air pollution particulate-mediated oxidant stress in alveolar macrophages. *J. Toxicol. Environ. Health A 54*, 529−545.

(8) Terada, N., Hamano, N., Maesako, K. I., Hiruma, K., Hohki, G., Suzuki, K., and et al. (1999) Diesel exhaust particulates upregulate histamine receptor mRNA and increase histamine-induced IL-8 and GM-CSF production in nasal epithelial cells and endothelial cells. *Clin. Exp. Allergy 29*, 4−8.

(9) Barrett, E. G., Johnston, C., Oberdörster, G., and Finkelstein, J. N. (1999) Silica-induced chemokine expression in alveolar type II cells is mediated by TNF-alpha-induced oxidant stress. *Am. J. Physiol. 276*, L979−L988.
(10) Donaldson, K., Brown, G. M., Brown, D. M., Slight, J., Robertson, M. D., and Davis, J. M. (1990) Impaired chemotactic responses of bronchoalveolar leukocytes in experimental pneumoconiosis. *J. Pathol. 160*, 63−69.
(11) Callis, A. H., Sohnle, P. G., Mandel, G. S., Wiessner, J., and Mandel, N. S. (1995) Kinetics of inflammatory and fibrotic pulmonary changes in a murine model of silicosis. *J. Lab. Clin. Med. 105*, 547−553.
(12) Clarke, R. W., Catalano, P. J., Koutrakis, P., Murthy, G. G., Sioutas, C., Paulauskis, J., and et al. (1999) Urban air particulate inhalation alters pulmonary function and induces pulmonary inflammation in a rodent model of chronic bronchitis. *Inhalation Toxicol. 11*, 637−656.
(13) Nightingale, J. A., Maggs, R., Cullinan, P., Donnelly, L. E., Rogers, D. F., Kinnersley, R., and et al. (2000) Airway inflammation after controlled exposure to diesel exhaust particulates. *Am. J. Respir. Crit. Care Med. 162*, 161−166.
(14) Calderón-Garcidueñas, L., Mora-Tiscareño, A., Fordham, L. A., Chung, C. J., García, R., Osnaya, N., and et al. (2001) Canines as sentinel species for assessing chronic exposures to air pollutants: Part 1. Respiratory pathology. *Toxicol. Sci. 61*, 342−355.
(15) Lies, K. H., Hartung, A., Postulka, A., Gring, H., and Schulze, J. (1986) Composition of diesel exhaust with particular reference to particle bound organics including formation of artifacts. *Dev. Toxicol. Environ. Sci. 13*, 65−82.
(16) Borm, P. J. A. (1997) Toxicity and occupational health hazards of coal fly ash (CFA). A review of data and comparison to coal mine dust. *Ann. Occup. Hyg. 41*, 659−676.
(17) Lee, S. W. (2001) Source profiles of particulate matter emissions from a pilot-scale boiler burning North American coal blends. *J. Air Waste Manage. Assoc. 11*, 1568−1578.
(18) Jiang, N., Dreher, K. L., Dye, J. A., Li, Y., Richards, J. H., Martin, L. D., and et al. (2000) Residual oil fly ash induces cytotoxicity and mucin secretion by guinea pig tracheal epithelial cells via an oxidant-mediated mechanism. *Toxicol. Appl. Pharmacol. 163*, 221−230.
(19) Gilmour, M. I., Daniels, M., McCrillis, R. C., Winsett, D., and Selgrade, M. J. K. (2001) Air pollutant-enhanced respiratory disease in experimental animals. *Environ. Health Perspect. 109*, 619−622.
(20) Fubini, B., Fenoglio, I., Elias, Z., and Poirot, O. (2001) Variability of biological responses to silicas: effect of origin, crystallinity, and state of surface on generation of reactive species and morphological transformation of mammalian cells. *J. Environ. Pathol. Toxicol. Oncol. 20*, 95−108.
(21) Sedmak, D. D., Roberts, W. H., Stephens, R. E., Buesching, W. J., Morgan, L. A., Davis, D. H., and et al. (1990) Inability of cytomegalovirus infection of cultured endothelial cells to induce HLA class II antigen expression. *Transplantation 49*, 458−462.
(22) Maciag, T., Cerundolo, J., Ilsley, S., Kelley, P. R., and Forand, R. (1979) An endothelial cell growth factor from bovine hypothalamus: Identification and partial characterization. *Proc. Natl. Acad. Sci. U.S.A. 76*, 5674−5678.
(23) Boyum, A. (1968) Separation of leukocytes from blood and bone marrow. *Scand. J. Clin. Lab. Invest. 21*, 77−89.
(24) Johnson, S. A., Brigham, E. S., Ollivier, P. J., and Mallouk, T. E. (1997) Effect of micropore topology on the structure and properties of zeolite polymer replicas. *Chem. Mater. 9*, 2448−2458.
(25) Seah, M. P. (1983) Quantification of AE and XPS. In *Practical Surface Analysis by Auger and X-ray Photoelectron Spectroscopy* (Briggs, D., and Seah, M. P., Eds.) pp 181−214, John Wiley & Sons, New York.
(26) Yan, L., Gupta, R. P., and Wall, T. F. (2002) A mathematical model of ash formation during pulverized coal combustion. *Fuel 81*, 337−344.
(27) Alonso, C., Morato, A., Medina, F., Guirado, F., Cesteros, Y., Salagre, P., Sueiras, J. E., Terrado, R., and Giralt, A. (2000) Preparation and Characterization of different phases of aluminum trifluoride. *Chem. Mater. 12*, 1148−1155.
(28) Saadoun, M., Bessais, B., Mliki, N., Ferid, M., Ezzaouia, H., and Bennaceur, R. (2003) Formation of luminescent $(NH_4)_2SiF_6$ phase from vapor etching-based porous silicon. *Appl. Surf. Sci. 210*, 240−248.
(29) Pober, J. S., and Cotran, R. S. (1991) Cytokines and endothelial cell biology. *Physiol. Rev. 70*, 427−451.
(30) Knight, D. A., Waldman, W. J., and Sedmak, D. D. (1997) Human cytomegalovirus does not induce human leukocyte antigen class II expression on arterial endothelial cells. *Transplantation 63*, 1366−1369.
(31) Knight, D. A., Waldman, W. J., and Sedmak, D. D. (1999) Cytomegalovirus-mediated modulation of adhesion molecule expression by human arterial and microvascular endothelial cells. *Transplantation 68*, 1814−1818.
(32) Oberdörster, G., Ferin, J., Gelein, R., Soderholm, S. C., and Finkelstein, J. (1992) Role of the alveolar macrophage in lung injury: Studies with ultrafine particles. *Environ. Health Perspect. 97*, 193−199.
(33) Jutila, M. A., Berg, E. L., Kishimoto, T. K., Picker, L. J., Bargatze, R. F., Bishop, D. K., and et al. (1989) Inflammation-induced endothelial cell adhesion to lymphocytes, neutrophils, and monocytes. Role of homing receptors and other adhesion molecules. *Transplantation 48*, 727−731.
(34) Fubini, B., and Mollo, L. (1995) Role of iron in the reactivity of mineral fibers. *Toxicol. Lett. 82/82*, 951−960.
(35) Fach, E., Waldman, W. J., Williams, M., Long, J., Meister, R. K., and Dutta, P. K. (2002) Analysis of the biological and chemical reactivity of zeolite-based aluminosilicate fibers and particulates. *Environ. Health Perspect. 110*, 1087−1096.
(36) Donaldson, K., Brown, D. M., Mitchell, C., Dineva, M., Beswick, P. H., Gilmour, P., and MacNee, W. (1997) Free radical activity of PM_{10}: Iron-mediated generation of hydroxyl radicals. *Environ. Health Perspect. 105*, 1285−1289.
(37) Valavanidis, A., Salika, A., and Theodoropoulou, A. (2000) Generation of hydroxyl radicals by urban suspended particulate air matter. The role of iron ions. *Atmos. Environ. 34*, 2379−2386.
(38) She, H., Xiong, S., Lin, M., Zandi, E., Giulivi, C., and Tsudamoto, H. (2002) Iron activates NF-κB in Kupffer cells. *Am. J. Physiol. Gastrointest. Liver Physiol. 283*, G719−G726.
(39) Tsukamoto, H. (2002) Iron regulation of hepatic macrophage TNFα expression. *Free Radical Biol. Med. 32*, 309−313.
(40) Veronesi, B., de Haar, C., Lee, L., and Oortgiesen, M. (2002) The surface charge of visible particulate matter predicts biological activation in human bronchial epithelial cells. *Toxicol. Appl. Pharmacol. 178*, 144−154.
(41) Baxter, L. L. (1990) The evolution of mineral particle size distributions during early stages of coal combustion. *Prog. Energy Combust. Sci. 16*, 261−266.
(42) Smith, K. R., Vernath, J. M., Hu, A. A., Lightly, J. S., and Aust, A. E. (2000) Interleukin-8 Levels in human lung epithelial cells are increased in response to coal fly ash and vary with bioavailability of iron, as function of particle size and coal. *Chem. Res. Toxicol. 13*, 118−125.
(43) van Maanen, J., Borm, P. J. A., Knaapen, A., van Herwijnen, M., Schilderman, P. A. E. L., Smith, K. R., Aust, A. E., Tomatis, M., and Fubini, B. (1999) In vitro effects of coal fly ashes: Hydroxyl radical generation, iron release, and DNA damage and toxicity in rat lung epithelial cells. *Inhalation Toxicol. 11*, 1123−1141.
(44) Veranth, J. M., Smith, K. R., Hu, A. A., Lighty, J. S., and Aust, A. E. (2000) Mobilization of iron from coal fly ash was dependent upon particle size and source of coal: Analysis of rates and mechanisms. *Chem. Res. Toxicol. 13*, 382−389.
(45) Hochella, M. F., Jr. (1993) Surface chemistry, structure, and reactivity of hazardous mineral dust. In *Reviews in Mineralogy, Vol. 28, Health Effects of Mineral Dusts* (Guthrie, G. D., Jr., and Mossman, B. T., Eds.) pp 275−305, Mineralogical Society of America, Washington, DC.
(46) Addy, R. A., and Gilbert, B. C. (1995) Iron−ligand interactions and the Fenton reaction. In *Handbook of Metal−Ligand Interactions in Biological Fluids. Vol 2. Bioinorganic Chemistry* (Berthon, G., Ed.) pp 857−866, Marcel-Dekker, NY.

TX049893P